LASER & PHOTONICS REVIEWS

www.lpr-journal.org

Photonic Spin-Hall Effect at Generic Interfaces

Xiaohui Ling, Zan Zhang, Zhiping Dai, Zhiteng Wang, Hailu Luo, and Lei Zhou**

Although the photonic spin-Hall effect (PSHE) at optical interfaces has been widely studied in past years, its physical origin remains obscure. Here, through studying the scatterings of circularly polarized beams obliquely incident on a series of junctions linking two homogenous optical media, how the physical origin of the PSHE evolves as the interface changes from a slowly varying junction to a step-like sharp one is explored. Beams transmitted through a generic interface consist of two modes, a spin-maintained normal mode carrying a spin-redirection Berry (SRB) phase and a spin-flipped abnormal mode exhibiting a Pancharatnam–Berry (PB) phase. Under linear-polarization incidence, a spin-polarized beam transmitted through each junction is generally an interference of normal and abnormal modes corresponding to two different incident circular polarizations, and thus the resulting PSHE is dictated by the interplay and competition between two effects dictated by SRB and PB phases, respectively. Shrinking the interfacial region can increase the strength of the abnormal mode, making the measured PSHE change from the SRB-dominated one to the PB-dominated one. The results establish a unified framework to understand the PSHE at generic interfaces, offering practical ways to control the PSHE by "designing" the abnormal scatterings on optical interfaces.

1. Introduction

Photonic spin-Hall effect (PSHE) denotes the spin (helicity)-dependent shift of light-beam center along with certain optical processes where light beam changes its propagation direction.[1–6] In recent years, the PSHE has attracted intensive attention since it reveals the profound interplays between photonic angular momenta related to spin and orbit degrees of freedom and exhibits promising applications in precision measurement,[7–10] sensing,[11–13] image-edge detection,[14–16] and spin-optical devices.[17–22]

Many theories were developed to understand the PSHEs occurring in different circumstances.[1–6] In earlier days, researchers discovered that, as a linearly polarized light beam passes through a smoothly varying gradient-index medium (GIM) or an optical fiber, it can split into two circularly polarized light beams with opposite transverse-coordinate shifts in real space.[23–25] These effects belong to one type of PSHE, dictated by the spin-redirection-Berry (SRB) phase[26,27] gained by a spin-polarized light beam adiabatically changing its propagation direction. The SRB phase shares the same physics with the geometric phase gained by a quantum spin driven by a magnetic field slowly varying in time, discussed in the original seminar paper by Berry.[28] Later, scientists continued to study the PSHEs as light beams strike sharp optical interfaces, including single optical interfaces and multilayer films.[1–6,29–33] Initially, Onoda et al.[1] studied such effect using a semi-classical theory of light beam, based on essentially the concept of SRB phase in the refraction process. Two years later, the semi-classical theory was challenged by Bliokh et al.,[2,3] since light scatterings at sharp interfaces are not adiabatic processes and thus cannot be well described by the semi-classical theory. In contrast, the authors proposed a wave-theory to study the PSHE as an obliquely incident light beam strikes the sharp optical interface, based on Fresnel coefficients derived in matching electromagnetic boundary conditions at the interfaces. However, although the formulas given by Bliokh et al. are accurate,[2,3] confirmed later by Hosten et al.[4] in a carefully designed experiment, the intrinsic physics is buried inside the rigorous formulas. For example, it is not clear whether the SRB phase still plays an important role in such optical process, or whether there are new mechanisms to govern the PSHE.

In a parallel line, another spin–orbit-coupling-induced effect drew much research attention related to light scatterings at sharp optical interfaces. In 2012, Yavorsky et al.[34] discovered that, as a circularly polarized beams is scattered by a sharp optical interface under normal incidence, each k component inside the

X. Ling, Z. Zhang, Z. Dai, Z. Wang
Laboratory for Spin-Orbit Photonics
College of Physics and Electronic Engineering
Hengyang Normal University
Hengyang 421002, China
E-mail: xhling@hynu.edu.cn

X. Ling, L. Zhou
State Key Laboratory of Surface Physics
Key Laboratory of Micro and Nano Photonic Structures (Ministry of Education) and Physics Department
Fudan University
Shanghai 200433, China
E-mail: phzhou@fudan.edu.cn

H. Luo
Laboratory for Spin Photonics
School of Physics and Electronics
Hunan University
Changsha 410082, China

The ORCID identification number(s) for the author(s) of this article can be found under https://doi.org/10.1002/lpor.202200783

DOI: 10.1002/lpor.202200783

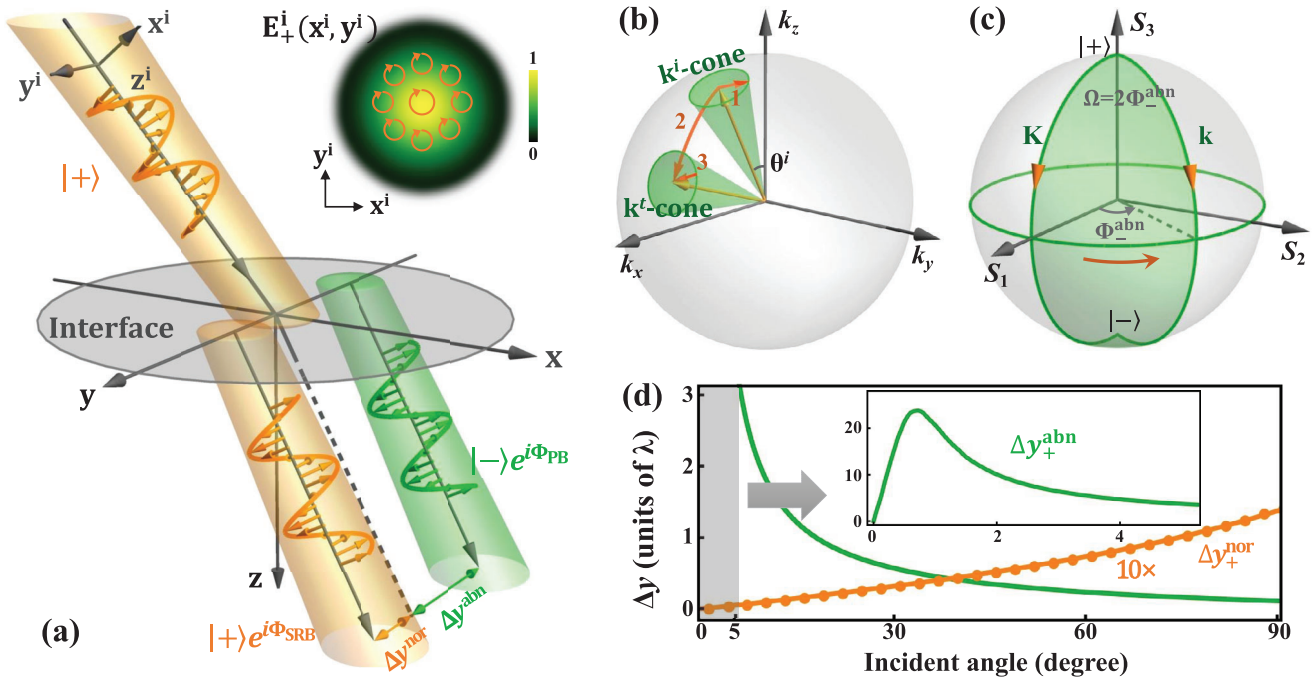

Figure 1. Two types of geometric Berry phase and spin-Hall shifts in light beam refraction at a sharp interface. a) Schematic of a circularly polarized light beam refracted at a sharp interface. The refracted beam has a spin-maintained normal component carrying an SRB phase (Φ_{SRB}) with an transverse shift of Δy^{nor} and a spin-reversal abnormal one with a PB phase (Φ_{PB}) exhibiting a shift of Δy^{abn}. Inset: Intensity and circular-polarization distribution of the incident beam. b,c) Schematic representation of the SRB phase in k space and the PB phase on Poincaré sphere, respectively. When the spin polarized wave with k^i is refracted to (or smoothly varied to) that with k^t, an SRB phase is obtained. A PB phase is gained as a spin-up plane wave with k undergoes a spin-reversed scattering, which is half of the solid angle Ω of the shaded area surrounded by two paths connecting the north and south poles on the Poincaré sphere. d) Calculation of the beam shifts of normal mode (orange line) and abnormal mode (green line) in a single interface with $n_i = 1$ and $n_t = 2$. Geometrical-optics calculation (see the Supporting Information) of the shift in a GIM with smoothly varying refractive index from 1 to 2 is shown by orange dots. 10×: Data of the normal-mode shift are magnified by 10 times.

beam can gain a k-dependent phase in the spin-converted scattering process, resulting in an optical vortex with a topological charge of ±2.[35,36] Recently, a full-wave theory is developed to revisit the spin-orbit couplings at sharp optical interfaces under both normal and off-normal incidences.[37] It is revealed that such k-dependent phases are actually of the Pancharatnam–Berry (PB) origin,[28,38–43] being another type of geometric Berry phase gained by light in spin-converted scattering processes.[35–37] In addition, the authors also pointed out that such PB phase plays a very important role in determining the spin-Hall shift of light at off-normal incidence, in addition to the SRB phase previously discussed. Given different Berry phases (e.g., SRB phase and PB phase) appearing in different optical processes, it is natural to ask what are the exact roles played by different Berry phases and how they interplay and compete in these optical processes.

In this paper, we answer these questions through studying the scatterings of circularly polarized light beams on a series of junctions (exhibiting different spatially varying refraction-index profiles) linking two homogenous optical media. We find that the beam transmitted through a generic optical interface is composed of a spin-maintained normal mode carrying an SRB phase and a spin-flipped abnormal mode carrying a PB phase. Therefore, under linear-polarization incidence, a certain spin-component of the transmitted beam must be a superposition of a normal mode and an abnormal mode corresponding to different incident circular polarizations. As the junction evolves continuously from a GIM to a sharp interface, the strength of the abnormal mode inside the transmitted beam increases which enhances the importance of the PB mechanism in determining the PSHE. Finally, we discuss how to enhance the role played by the PB mechanism in determining the PSHE at optical processes, and proposed one possible solution of employing carefully designed metamaterial slabs to increase the abnormal-mode generation efficiency.

2. Full-Wave Theory for the PSHE at Generic Interfaces

2.1. Full-Wave Theory for the PSHE at a Single Interface

Figure 1a shows the principal illustration of a circularly polarized light beam refracted at a single interface. We define (x, y, z) and (x^a, y^a, z^a) as the laboratory and local coordinate systems, respectively, where $y \parallel y^a$ and z^a is parallel to the propagation direction of the light beam. The superscripts $a = \{i,t\}$ label the incident and transmitted light, respectively. Because of the same physics shared by the reflection and transmission, we here only consider the transmission case for the sake of simplicity. A finite-width light beam is a coherent superposition of many plane waves with slightly different propagation directions, each of which has different angle and plane of incidence. In the spin basis (circular

polarization basis), we represent the electric filed of a light beam in an arbitrary transverse plane (z^a = const.) as

$$\mathbf{E}_{\perp}^{a}(\mathbf{r}_{\perp}^{a}, z^{a}) = \int d^{2}\mathbf{k}_{\perp}^{a} e^{i\mathbf{k}^{a}\cdot\mathbf{r}^{a}} \sum_{\sigma=+,-} \tilde{E}_{\sigma}^{a}(\mathbf{k}^{a})\hat{\mathbf{e}}_{\sigma}^{a} \tag{1}$$

where $\mathbf{k}^a$ and $\mathbf{r}^a$ are the wave-vector and position vector in the local coordinate, $\mathbf{k}^a \cdot \mathbf{r}^a = \mathbf{k}_{\perp}^a \cdot \mathbf{r}_{\perp}^a + k_z^a z^a = k_x^a x^a + k_y^a y^a + k_z^a z^a$ with $k_z^a = [(k^a)^2 - (k_{\perp}^a)^2]^{1/2}$, and $\hat{\mathbf{e}}_{\sigma}^{a} = (\hat{\mathbf{x}}^a + i\sigma\hat{\mathbf{y}}^a)/\sqrt{2}$.

Recently, we have established a 2×2 matrix $\mathbf{M}^{(t)}$ to connect the transmitted and incident beam,[37] i.e.,

$$\begin{bmatrix} \tilde{E}_{+}^{t}(\mathbf{k}^{t}) \\ \tilde{E}_{-}^{t}(\mathbf{k}^{t}) \end{bmatrix} = \mathrm{M}^{(t)} \begin{bmatrix} \tilde{E}_{+}^{i}(\mathbf{k}^{i}) \\ \tilde{E}_{-}^{i}(\mathbf{k}^{i}) \end{bmatrix} = \begin{pmatrix} M_{++} & M_{+-} \\ M_{-+} & M_{--} \end{pmatrix} \begin{bmatrix} \tilde{E}_{+}^{i}(\mathbf{k}^{i}) \\ \tilde{E}_{-}^{i}(\mathbf{k}^{i}) \end{bmatrix} \tag{2}$$

Assume that the incident beam is a left-handed circular-polarization Gaussian one with **E**-field distribution on its waist plane being (see Figure 1a inset)

$$\mathbf{E}_{+}^{i}(\mathbf{r}_{\perp}^{i}) = \exp[-(r_{\perp}^{i}/w_0)^2]\hat{\mathbf{e}}_{+}^{i}, \tag{3}$$

with w_0 being the half-width of the beam waist. Substituting Equation (3) into Equation (1) we obtain $\tilde{E}_{+}^{i}(\mathrm{k}^{i}) = \frac{w_0^2}{2}\exp[-(k_{\perp}^{i}w_0)^2/4]$ and $\tilde{E}_{-}^{i}(\mathrm{k}^{i}) \equiv 0$. Putting $\tilde{E}_{\pm}^{i}(\mathrm{k}^{i})$ into Equation (2) to get $\tilde{E}_{\pm}^{t}(\mathrm{k}^{t})$, we have the transmitted **E**-fields as

$$\begin{aligned} E_{++}^{\mathrm{t}}(\mathbf{r}_{\perp}^{\mathrm{t}}) &= \int d^{2}\mathrm{k}_{\perp}^{\mathrm{t}} e^{i\mathbf{k}^{\mathrm{t}}\cdot\mathbf{r}^{\mathrm{t}}} M_{++}\tilde{E}_{+}^{\mathrm{i}}(\mathbf{k}^{\mathrm{i}}) \\ E_{-+}^{\mathrm{t}}(\mathbf{r}_{\perp}^{\mathrm{t}}) &= \int d^{2}\mathrm{k}_{\perp}^{\mathrm{t}} e^{i\mathbf{k}^{\mathrm{t}}\cdot\mathbf{r}^{\mathrm{t}}} M_{-+}\tilde{E}_{+}^{\mathrm{i}}(\mathbf{k}^{\mathrm{i}}) \end{aligned} \tag{4}$$

Here, the spin-maintained and spin-reversal beams are separately called *normal* and *abnormal* modes. This indicates that even the incident beam exhibits a pure spin, the refracted beam can still include a spin-flipped abnormal component (see Figure 1a) which comes from the "effective anisotropy" possessed by the optical interface at oblique incidence [i.e., $t_{+-} = (t_{\mathrm{p}} - t_{\mathrm{s}})/2 \neq 0$]. When the incident beam is a right-handed circular-polarization one, one can also obtain the normal and abnormal modes in the refraction, i.e., $E_{--}^{t}(\mathbf{r}_{\perp}^{t})$ and $E_{-+}^{t}(\mathbf{r}_{\perp}^{t})$, akin to Equation (4). The centroid shifts of the normal and abnormal modes (Δy^{nor} and Δy^{abn}) can be directly computed as the expectation values of the transverse position of the beam:[44,45]

$$\Delta\, y^{\mathrm{nor,abn}} = \frac{\iint y^{\mathrm{t}} \left|E^{\mathrm{nor,abn}}\right|^2 dx^{\mathrm{t}} dy^{\mathrm{t}}}{\iint \left|E^{\mathrm{nor,abn}}\right|^2 dx^{\mathrm{t}} dy^{\mathrm{t}}} \tag{5}$$

2.2. Two Kinds of Berry Phase and Beam Shifts

We have recently demonstrated that the abnormal mode exhibits an intriguing topological phase transition from vortex generation at normal incidence to PSHE under oblique incidence.[37] Here we are only interested in the latter. Then, under paraxial-wave approximations, we have the simplified form of $\mathbf{M}^{(t)}$ as

$$\mathbf{M}^{(t)} \approx \begin{bmatrix} t_{++}\exp(i\Phi_{+}^{\mathrm{nor}}) & t_{+-}\exp(i\Phi_{-}^{\mathrm{abn}}) \\ t_{-+}\exp(i\Phi_{+}^{\mathrm{abn}}) & t_{--}\exp(i\Phi_{-}^{\mathrm{nor}}) \end{bmatrix} \tag{6}$$

where $t_{++} = t_{--} = (t_p + t_s)/2$ and $t_{+-} = t_{-+} = (t_p - t_s)/2$ are Fresnel transmission coefficients of the central plane waves within the beam in the spin basis, and

$$\begin{aligned} \Phi_{\sigma}^{nor} &= \frac{(\sigma\cos\theta^{i} - \sigma^{nor}\cos\theta^{t})k_y}{k_0\sin\theta^{i}} \\ \Phi_{\sigma}^{abn} &= \frac{(\sigma\cos\theta^{i} - \sigma^{abn}\cos\theta^{t})k_y}{k_0\sin\theta^{i}} \end{aligned} \tag{7}$$

The normal-mode phase Φ_{σ}^{nor} is an SRB phase which can be further written as $\Phi_{\sigma}^{nor} = \sigma(\cos\theta^{i} - \cos\theta^{t})k_y/(k_0\sin\theta^{i})$ due to the spin unchanged in the normal mode, i.e., $\sigma^{nor} = \sigma$ ($\sigma, \sigma^{nor,abn} \in \{+,-\}$). It can be represented by a direction sphere in the momentum space (Figure 1b). The k-cone of the incident beam (k^{i}-cone) changes to that of the refracted beam (k^{t}-cone) after refraction. This process is not continuous and therefore we only need to consider the phase difference between the initial and final states as Φ_{σ}^{nor}. For a GIM, the evolution is continuous, and the geometric phase also takes the same form.

The abnormal-mode phase Φ_{σ}^{abn} can be further expressed as $\Phi_{\sigma}^{abn} = \Phi_{\sigma}^{nor} + 2\sigma k_y\cos\theta^{t}/(k_0\sin\theta^{i})$ due to spin flip ($\sigma^{abn} = -\sigma$), which are divided into two parts, one equal to the SRB phase in the normal mode, and the other with a factor of 2 originating from the spin reversal of the abnormal mode, i.e., a momentum-dependent PB phase which dominates in the abnormal mode. Such PB phase can be geometrically represented by a Poincaré sphere (Figure 1c) where the polarization state evolves from the north (south) pole to the south (north) pole.[37,42,43,46,47] This evolution is also not continuous, and we also need to consider only the phase difference between the initial and final states. In fact, when the propagation direction of the beam is unchanged, such as a thin slab placed in air, the SRB phase vanishes, and only the PB phase remains.

The geometric phase of either the normal or abnormal mode is a linear function of k_y, which forms a linear phase gradient in momentum space, leading to real-space beam shifts:[6,32,48]

$$\begin{aligned} \Delta y_{\sigma}^{\mathrm{nor}} &= -\nabla_{k_y}\Phi_{\sigma}^{\mathrm{nor}} = \sigma\frac{\cos\theta^{\mathrm{t}} - \cos\theta^{\mathrm{i}}}{k_0\sin\theta^{\mathrm{i}}} \\ \Delta y_{\sigma}^{\mathrm{abn}} &= -\nabla_{k_y}\Phi_{\sigma}^{\mathrm{abn}} = -\sigma\frac{\cos\theta^{\mathrm{t}} + \cos\theta^{\mathrm{i}}}{k_0\sin\theta^{\mathrm{i}}} \end{aligned} \tag{8}$$

For an optically thin slab placed in a homogenous media, the refracted beam is not deflected with respect to the incident one, so the normal-mode shift is vanishing and only the abnormal-mode one remains. At near-normal incidence, Equation (8) is no longer valid and the full theory (Equations (1)–(5)) must be employed. And then the beam intensity pattern of the abnormal mode is severely distorted and exhibits an intriguing topological phase transition from vortex generation to the PSHE. We visualized the shifts of the two modes in Figure 1d for a single interface composed of two semi-infinite media with their refractive indices being n_{i} and n_{t}, respectively.

Because of the rotational symmetry of the interface with respect to the z direction, the total angular momentum of the normal and abnormal modes in this direction must be

conserved, respectively. The geometric phases of the normal and abnormal modes (Equation (7)) indicate the change of the spin angular momentum in the z direction upon refraction, i.e., $\Delta L^{nor} = \sigma \cos\theta^i - \sigma^{nor}\cos\theta^t$ and $\Delta L^{abn} = \sigma\cos\theta^i - \sigma^{abn}\cos\theta^t$, where $\sigma\cos\theta^i$, $\sigma^{nor}\cos\theta^t$, and $\sigma^{abn}\cos\theta^t$ are averaged spin angular momentum per photon of the incident beam, the normal and abnormal modes, respectively. In fact, due to the angular momentum conservation, $\Delta L^{nor,abn}$ will convert into orbital angular momentum which manifests as the centroid shifts of the normal and abnormal modes, namely, $\Delta y_\sigma^{nor,abn} = \Delta L^{nor,abn}/P_x$, where $P_x = k_0 \sin\theta^i$ is averaged linear momentum per photon in the *x*-direction. The spin-Hall shifts calculated in this approach are in perfect agreement with Equation (8). Therefore, it is clear that the SRB and PB phases naturally involve the law of angular momentum conservation, and through which one can directly derive the shifts of the normal and abnormal modes.

We now introduce the formula derived above to reanalyze the PSHE in the existing work under linear polarization irradiation, e.g., horizontal polarization (*H* or *p* polarization) and vertical polarization (*V* or *s* polarization). Assuming that the incident beam is *H*-polarized, it contains an equal weight of left- and right-handed circular polarization components, i.e., $\tilde{E}^i_+(\mathrm{k}^i) = \tilde{E}^i_-(\mathrm{k}^i)$. Substituting this condition into Equations (1) and (2), we obtain the transmitted beam as

$$\begin{aligned} E^{\mathrm{t}}_+(\mathbf{r}^{\mathrm{t}}_\perp) &= E^{\mathrm{t}}_{++}(\mathbf{r}^{\mathrm{t}}_\perp) + E^{\mathrm{t}}_{+-}(\mathbf{r}^{\mathrm{t}}_\perp) \\ E^{\mathrm{t}}_-(\mathbf{r}^{\mathrm{t}}_\perp) &= E^{\mathrm{t}}_{-+}(\mathbf{r}^{\mathrm{t}}_\perp) + E^{\mathrm{t}}_{--}(\mathbf{r}^{\mathrm{t}}_\perp) \end{aligned} \tag{9}$$

It is found that the left and right-handed components of the transmitted beam are the interference and superposition of a normal mode with an SRB phase and an abnormal mode with a PB phase. For an interface composed of natural materials, such as air–glass interface, the strength of the abnormal mode is generally far less than that of the normal mode, and the shift of $E^t_\pm(\mathbf{r}^t_\perp)$ is mainly determined by the normal mode.

2.3. Extending the PSHE Theory to Generic Interfaces

We have given a full-wave theory above to describe the PSHE at a single interface. We arrived at an important conclusion: the change of the beam propagation direction due to the refractive index change can produce a normal mode carrying an SRB phase with an SRB-induced shift; the spin reversal caused by the effective anisotropy of the *p*- and *s*-wave components inside the beam can generate an abnormal mode carrying a momentum-dependent PB phase with a PB-induced shift. The two kinds of geometric phase have different mechanisms, which together dominate the PSHE at an optical interface. One can also see that the normal-mode shift and abnormal-mode shift depend upon their respective geometric phases, and their efficiency is determined by the Fresnel coefficients ($t_{++,--}$ and $t_{-+,+-}$). Therefore, it is easy to extend the PSHE theory from a single interface to generic junctions or interfaces, such as multilayer film stacks.

We now consider a junction or a complex interface consisting of a *m*-layer film stack. On one hand, the beam shift generated by any single interface within the junction can be computed according to Equation (8). Then, the final shifts generated by the junction are the sum of the shifts at each single interface, i.e.,

$$\begin{aligned} \Delta y_\sigma^{nor} &= \sum_{\xi=1}^{m} \sigma \frac{\cos\theta^{\xi+1} - \cos\theta^{\xi}}{k_\xi \sin\theta^\xi} = \sigma \frac{\cos\theta^t - \cos\theta^i}{k_0 \sin\theta^i} \\ \Delta y_\sigma^{abn} &= -\sum_{\xi=1}^{m} \sigma \frac{\cos\theta^{\xi+1} + \cos\theta^{\xi}}{k_\xi \sin\theta^\xi} = -\sigma \frac{\cos\theta^t + \cos\theta^i}{k_0 \sin\theta^i} \end{aligned} \tag{10}$$

where the denominator $k_\xi \sin\theta^\xi$ keeps constant for any interface within the junction according to the Snell's law. Obviously, one finds that these two equations, respectively, produce the same shifts as the normal and abnormal modes of a light beam refracted at a single interface (Equation (8)) when the two systems deflect the beam at a same angle. On the other hand, the efficiency of the normal and abnormal modes, respectively, $\eta^{nor} \approx |t_{++,--}|^2 = |t_p + t_s|^2/4$ and $\eta^{abn} \approx |t_{-+,+-}|^2 = |t_p - t_s|^2/4$, can be easily obtained by calculating the Fresnel coefficients of the film stack.

3. Discussion on the PB-Dominated PSHE

3.1. The Role of the PB Phase in the PSHE at a Generic Interface

Now a question arises: since the PSHE at a generic interface is dominated by the SRB phase and the PB phase together, can the weights of these two parts be adjusted by designing appropriate junctions? We first consider an extreme case, that is, an isotropic GIM connects two semi-infinite media with refractive indices of n_{i} and n_{t} (**Figure 2**a), respectively. Ideally, if the GIM has an extremely smooth change of the refractive index (i.e., thickness $h \to \infty$), a light beam can pass through the GIM without reflection, that is, $t_{\mathrm{p}} = t_{\mathrm{s}} = 1$. Hence, the transmitted beam has only a normal mode and no abnormal mode. This means the PSHE of the GIM is completely governed by the SRB phase. The beam shift generated by the GIM (Figure 1d, see the Supporting Information for details) is the same as the normal-mode shift of a single interface with abrupt change of refractive index from n_{i} to n_{t}. When shrinking the GIM, reflection occurs due to impedance mismatch of the interface, and t_{p} is no longer equal to t_{s}. Then the abnormal mode will appear. In the calculation, we can approximately divide the junction into an equal-thickness film stack with refractive index increment of $\Delta n = (n_{\mathrm{t}} - n_{\mathrm{i}})/m$ (Figure 2b). When the junction thickness vanishes (i.e., $h = 0$), it becomes a single interface (Figure 2c). Here we calculate the normalized efficiency of abnormal modes against the layer number *m* for several special incident angles, as shown in Figure 2d. We find that the efficiency of the abnormal mode increases oscillatorily when the junction shrinks, and reaches the maximum when the thickness of the junction is 0 (i.e., a single interface). However, the efficiency of the abnormal mode is still extremely weak (less than 1%).

3.2. PB-Dominated PSHE at a Slab Placed in a Homogeneous Medium

Note that when $\theta^i = \theta^t$, the normal-mode shift is $\Delta y_\sigma^{nor} = 0$ (see Equation (8)) with a non-vanishing weight (efficiency), and the

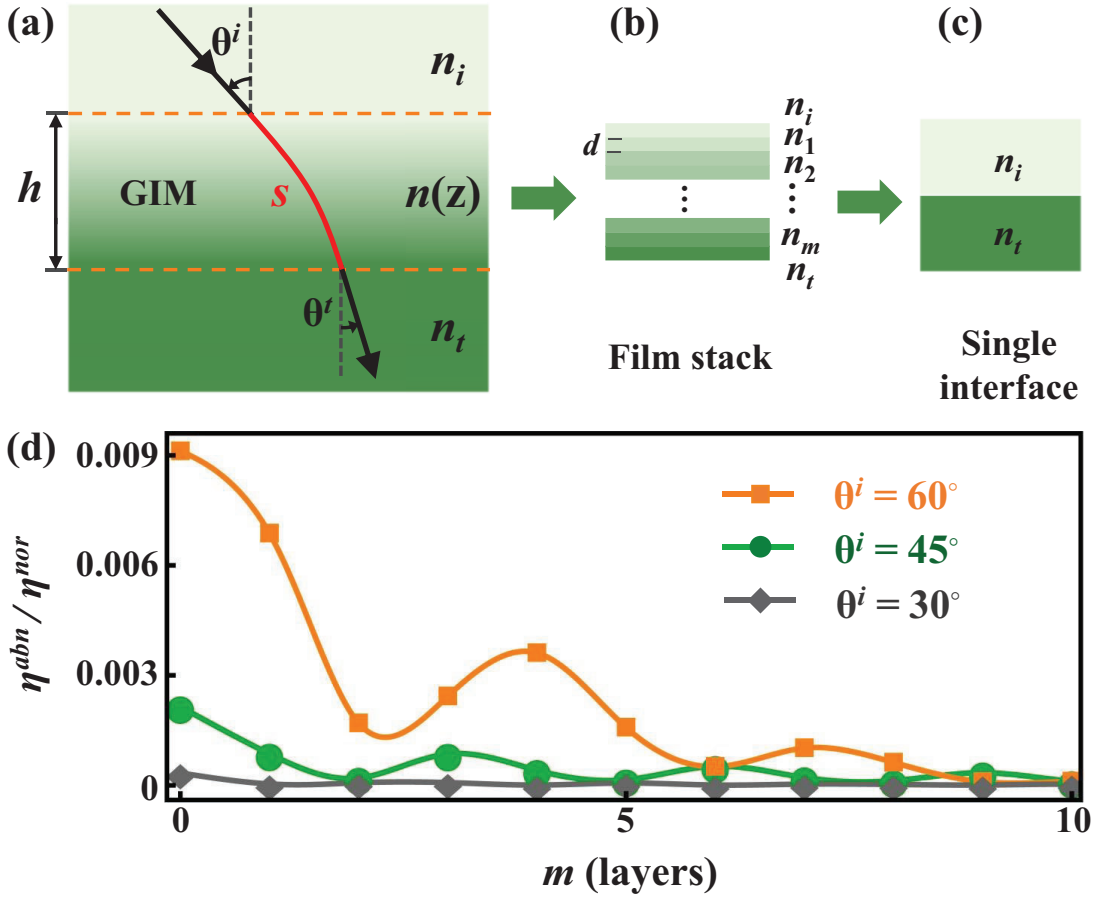

Figure 2. Abnormal-mode efficiency for a junction evolving from a GIM to a single interface. a) Schematic of a junction (e.g., a GIM) connecting two semi-infinite media with thickness h, and refractive indices n_i and n_t, respectively. b) The junction can be approximately divided into a m-layer film stack with equal thickness ($d = 0.5\lambda$) and refractive-index increment $\Delta n = (n_t - n_i)/m$. c) An extreme case ($h = 0$) of the junction, i.e., a single interface. d) The normalized efficiency is evaluated as the ratio of the abnormal- and normal-mode efficiencies.

PSHE is completely governed by the abnormal mode carrying a PB phase, as long as the refractive indices on both sides of a junction or an interface are equal (i.e., $n_i = n_t$). In this case, the abnormal-mode shift can be simplified as $\Delta\gamma_\sigma^{abn} = -2\sigma \cot\theta^i / k_0$. Such a typical junction is a slab placed in a homogeneous medium, which can be a single-layer film, a film stack, or even a GIM. No matter what the configuration is, it will not affect the shifts of the normal and abnormal modes, but only change the relative weights of the normal and abnormal modes.

Under linear polarization irradiation, the shift of each circular polarization component is actually the result of the interference and superposition between a normal mode with a high weight and a small shift and an abnormal mode with a small weight and a large shift. This picture can be illustrated in **Figure 3**a,b. By modulating the polarization of the incident light beam, the intensities of the normal and abnormal modes can be adjusted, so as to change the amplitude and direction of the measured shifts. Because of the interference and superposition, such shift is very sensitive to the polarization of the incident light. Typically, for a single interface, when a H- and a V-polarized beam illuminates a single interface, respectively, the shifts of the circular polarization component are obviously different (Figure 3c). For a slab whose PSHE is completely dominated by the PB phase, the shifts show greater difference and even have opposite signs. This also indicates that the PSHE completely dominated by the PB phase in a slab can have richer properties than those dominated by the SRB phase in a single interface.

In fact, the momentum-dependent PB phase plays an important role in the PSHE at a generic interface or junction, which has not been recognized for a long time. Only recently, people have begun to realize this.[37,46–48] However, the weight or the efficiency of the PB-phase-carrying abnormal mode is extremely weak (less than 10%) for a slab made of conventional materials (**Figure 4**a). This limits the capability to manipulate the PSHE with the PB phase. In what follows, we will propose some specially designed metamaterial slabs to significantly enhance the efficiency of the PB-phase-carrying abnormal mode.

3.3. Enhancing the Efficiency of the PB-Induced PSHE by ϵ_z-Near-Zero Uniaxial Slabs

From the above discussion, there is an interesting phenomenon that the normal mode has a tiny shift but a large efficiency (see

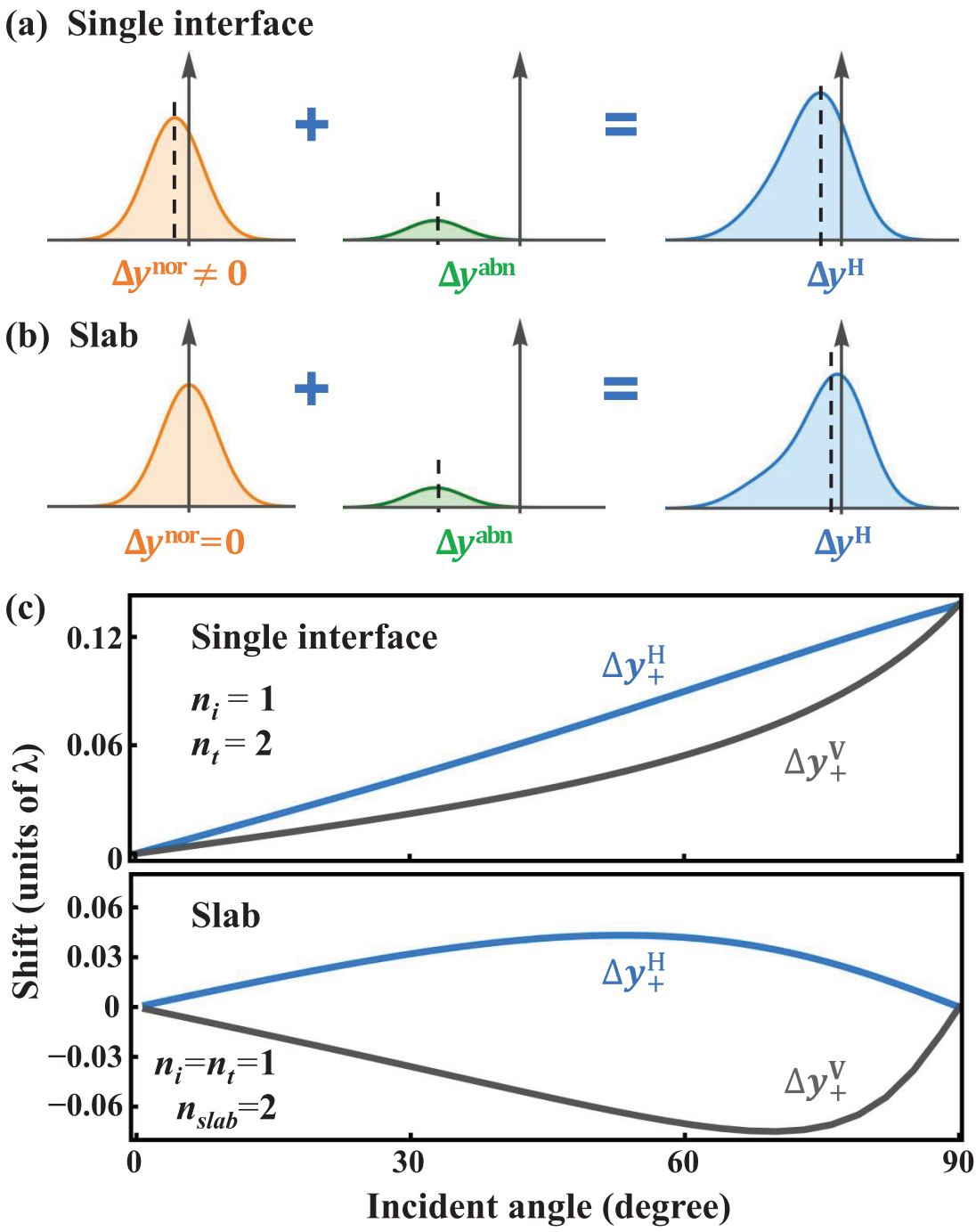

Figure 3. The PSHE under linear polarization illumination. The spin-Hall shift at a) a single interface and b) a slab, respectively, under linearly polarized incidence is illustrated as the superposition of a normal mode with a relatively large weight and a tiny shift and an abnormal mode with a small weight and a large shift. c) Calculated shifts under H- and V-polarized incidence at a single interface (upper) and a slab (lower).

Figure 2d), while the abnormal mode has a large shift but a small efficiency. Therefore, one may be curious to know whether we can significantly enhance the efficiency of the abnormal mode, even obtain nearly 100% efficiency. In fact, the efficiency can be enhanced so long as the effective anisotropy $|t_p - t_s|$ of the *p*- and *s*-polarized wave components within the beam is increased. For example, for an isotropic ϵ-near-zero slab, $|t_p|$ can reach 1 at some incident angles, while $|t_s|$ can be close to 0, bringing the efficiency up to ≈25% (Figure 4b). One can expect that if we can make one of t_p and t_s be 1 and the other −1, a 100%-efficiency of the abnormal mode could be achieved.

Anisotropic media have more degrees of freedom than isotropic ones and are expected to achieve a near-unity efficiency. We consider an optically thin uniaxial slab with thickness *h* and

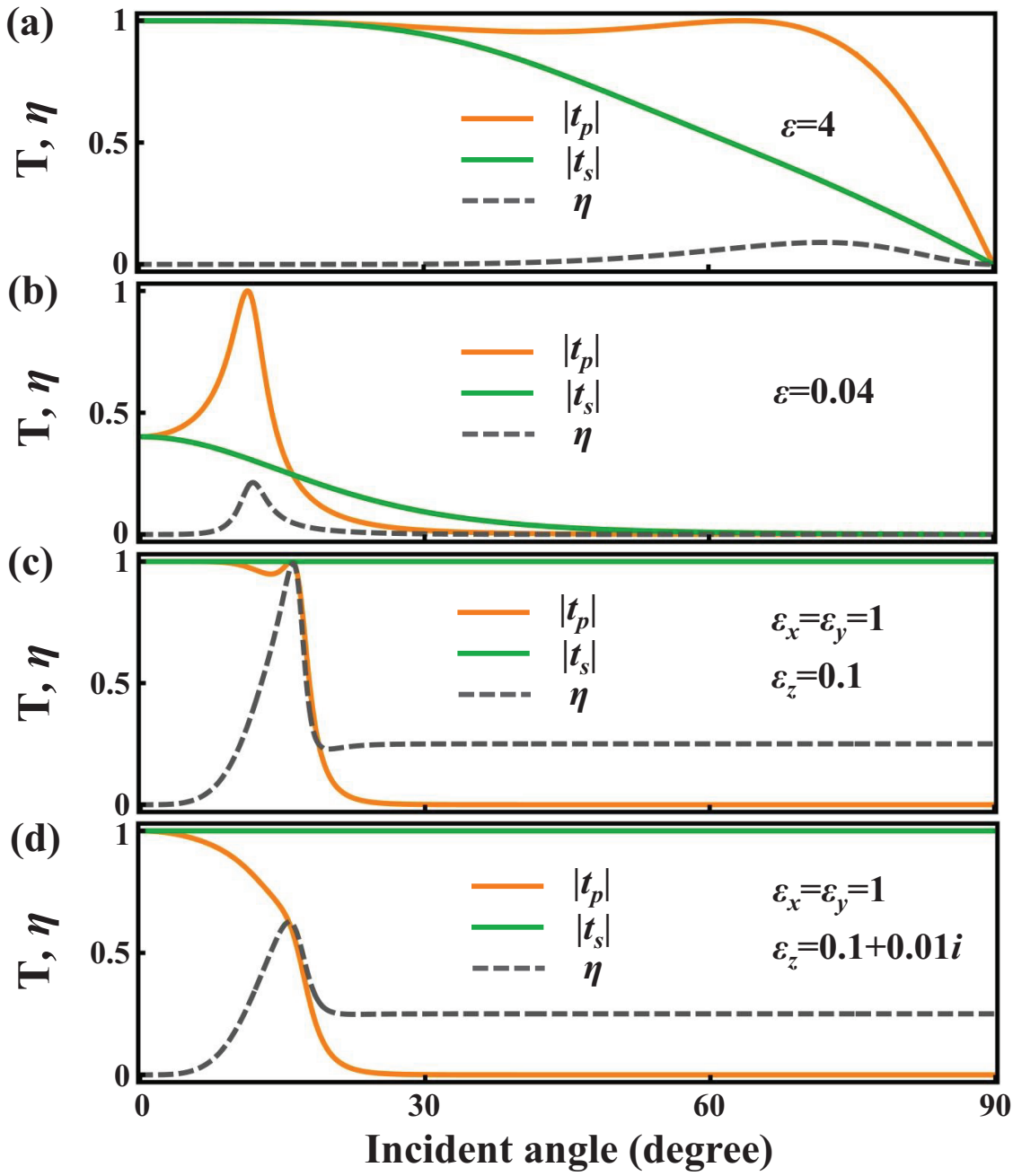

Figure 4. Enhancing the efficiency of the PB-induced SH shift. a) Transmission and efficiency of a conventional medium with $\epsilon = 4$. b) Transmission and efficiency of an ϵ-near-zero isotropic slab ($\epsilon = 0.04$). c) Transmission and efficiency of an ϵ_z-near-zero slab without loss ($\epsilon_z = 0.1$). d) Transmission and efficiency of an ϵ_z-near-zero slab with loss ($\epsilon_z = 0.1 + 0.01i$). Here, the thickness of the slabs is taken as $h = 1\lambda$.

a permittivity tensor of $\varepsilon = diag(\varepsilon_x, \varepsilon_y, \varepsilon_z)$ ($\varepsilon_x = \varepsilon_y \neq \varepsilon_z$) and permeability $\mu = 1$. That is, the optical axis of the uniaxial slab is parallel to the z-axis. In this case, all the theory above is still valid. Since such uniaxial material has two independent parameters, $\varepsilon_{x,y}$ and ε_z, it has more degrees of freedom compared to an isotropic slab.

To obtain nearly 100% efficiency for the abnormal mode, it is necessary to make one of t_p and t_s to be 1 and the other to be −1 (no reflection). First, let $\varepsilon_x = \varepsilon_y = 1$, the same as that of free space, which ensures the full transmission of the *s*-polarized wave at any angle of incidence, i.e., $|t_s| \equiv 1$. Next, by adjusting the thickness and ε_z of the slab, the Fabry–Perot resonance condition for *p*-polarized wave can be realized near some incident angles, so that $|t_p| = 1$, so it is possible to achieve 100% efficiency. For example, we set $\varepsilon_z \to 0$, so that the critical angle of total reflection (i.e., satisfying $\varepsilon_z = \sin^2\theta_c^i$) of *p*-polarized wave becomes small. When the incident angle is greater than the critical angle, we have $t_p = 0$ and $|t_p - t_s| = 1$, the conversion efficiency is $\eta \equiv 25\%$;

when it is less than the critical angle, the case of full transmission ($t_p = \pm 1$) may occur because of the Fabry–Perot resonance of the *p*-polarized wave, making the value of $|t_p - t_s|$ be 2 or 0, as well as any intermediate value between them. That is, it is possible to achieve 100% efficiency when the *p*-polarized wave satisfies the Fabry–Perot resonance condition (Figure 4c).

The transmission coefficients and conversion efficiency of a uniaxial thin layer are calculated for $\varepsilon_x = \varepsilon_y = 1$ and $\varepsilon_z = 0.1$. As shown in Figure 4c, $|t_s| \equiv 1$ for all incident angles; and the *p*-polarized wave undergoes total reflection ($|t_p| = 0$) at $\theta^i > 18.43°$. When $\theta^i > 18.43°$, Fabry–Perot resonance satisfies at some angles with $t_p = \pm 1$, so that the conversion efficiency reaches 100% near $\theta_i = 15°$. We further consider a uniaxial slab with loss, i.e., $\varepsilon_z = 0.1 + 0.01i$, which weakens the conversion efficiency (Figure 4d). By adjusting the real part of ε_z and the thickness of the slab, the incidence angle at which the peak efficiency occurs could be tunable. With the development of nanophotonics, the above uniaxial slabs could be achieved in practice with artificial metamaterial (e.g., hyperbolic metasurface[49–51]).

4. Conclusions

We have extended the PSHE theory from a single optical interface to generic optical interfaces, and found that a light beam transmitted through a generic optical interface is composed of a normal mode carrying an SRB phase and an abnormal mode carrying a PB phase. Hence, under linear-polarization illumination, a certain spin-component of the transmitted beam must be a superposition of a normal mode and an abnormal mode corresponding to different incident circular polarizations. It is further found that the momentum-dependent PB-phase plays a dominant role in the PSHE in an optically thin slab, but its efficiency is generally extremely low. We have proposed an ϵ_z-near-zero uniaxial slab to significantly enhance the efficiency of the PB-induced PSHE. Our study established a unified framework to understand the PSHE at generic interfaces, and provides feasible ways to manipulate the PSHE by "designing" the abnormal scattering at optical interfaces.

Supporting Information

Supporting Information is available from the Wiley Online Library or from the author.

Acknowledgements

This work was supported by the National Natural Science Foundation of China (Grant Nos. 12174091 and 11874142), the Scientific Research Fund of Hunan Provincial Education Department (18A341), and the Laboratory of Optoelectronic Control and Detection Technology of the institution of higher learning of Hunan Province.

Conflict of Interest

The authors declare no conflict of interest.

Data Availability Statement

The data that support the findings of this study are available from the corresponding author upon reasonable request.

Keywords

beam shifts, Berry phase, photonic spin-Hall effect

Received: October 16, 2022
Revised: November 21, 2022
Published online:

[1] M. Onoda, S. Murakami, N. Nagaosa, *Phys. Rev. Lett.* **2004**, *93*, 083901.
[2] K. Y. Bliokh, Y. P. Bliokh, *Phys. Rev. Lett.* **2006**, *96*, 073903.
[3] K. Y. Bliokh, Y. P. Bliokh, *Phys. Rev. E* **2007**, *75*, 066609.
[4] O. Hosten, P. Kwiat, *Science* **2008**, *319*, 787.
[5] K. Y. Bliokh, F. J. Rodríguez-Fortuño, F. Nori, A. V. Zayats, *Nat. Photonics* **2015**, *9*, 796.
[6] X. Ling, X. Zhou, K. Huang, Y. Liu, C.-W. Qiu, H. Luo, S. Wen, *Rep. Prog. Phys.* **2017**, *80*, 066401.
[7] X. Zhou, X. Ling, H. Luo, S. Wen, *Appl. Phys. Lett.* **2012**, *101*, 251602.
[8] X. Qiu, L. Xie, X. Liu, L. Luo, Z. Zhang, J. Du, *Opt. Lett.* **2016**, *41*, 4032.
[9] S. Chen, X. Ling, W. Shu, H. Luo, S. Wen, *Phys. Rev. Appl.* **2020**, *13*, 014057.
[10] R. Wang, J. Zhou, K. Zeng, S. Chen, X. Ling, W. Shu, H. Luo, S. Wen, *APL Photonics* **2020**, *5*, 016105.
[11] W. Zhu, H. Xu, J. Pan, S. Zhang, H. Zheng, Y. Zhong, J. Yu, Z. Chen, *Opt. Express* **2020**, *28*, 25869.
[12] J. Xiao, T. Tang, X. Liang, K. Liu, Y. Tang, J. Li, C. Li, *Phys. Lett. A* **2021**, *416*, 127692.
[13] A. Srivastava, A. K. Sharma, Y. K. Prajapati, *Chem. Phys. Lett.* **2021**, *774*, 138613.
[14] T. Zhu, Y. Lou, Y. Zhou, J. Zhang, J. Huang, Y. Li, H. Luo, S. Wen, S. Zhu, Q. Gong, M. Qiu, Z. Ruan, *Phys. Rev. Appl.* **2019**, *11*, 034043.
[15] J. Zhou, H. Qian, C. Chen, J. Zhao, G. Li, Q. Wu, H. Luo, S. Wen, Z. Liu, *Proc. Natl. Acad. Sci. USA* **2019**, *116*, 11137.
[16] J. Liu, Q. Yang, S. Chen, Z. Xiao, S. Wen, H. Luo, *Phys. Rev. Lett.* **2022**, *128*, 193601.
[17] J. Petersen, J. Volz, A. Rauschenbeutel, *Science* **2014**, *346*, 67.
[18] Z. Shao, J. Zhu, Y. Chen, Y. Zhang, S. Yu, *Nat. Commun.* **2018**, *9*, 926.
[19] G. Hu, X. Hong, K. Wang, J. Wu, H. Xu, W. Zhao, W. Liu, S. Zhang, F. Garcia-Vidal, B. Wang, P. Lu, C. W. Qiu, *Nat. Photonics* **2019**, *13*, 467.
[20] Z. Xie, T. Lei, H. Qiu, Z. Zhang, H. Wang, X. Yuan, *Photonics Res.* **2020**, *8*, 121.
[21] R. Jin, L. Tang, J. Li, J. Wang, Z. G. Dong, *ACS Photonics* **2020**, *7*, 512.
[22] L. Du, Z. Xie, G. Si, A. Yang, C. Li, J. Lin, G. Li, H. Wang, X. Yuan, *ACS Photonics* **2020**, *6*, 1840.
[23] V. S. Liberman, B. Y. Zel'dovich, *Phys. Rev. A* **1992**, *46*, 5199.
[24] K. Y. Bliokh, Y. P. Bliokh, *Phys. Lett. A* **2004**, *333*, 181.
[25] K. Y. Bliokh, A. Niv, V. Kleiner, E. Hasman, *Nat. Photonics* **2008**, *2*, 748.
[26] R. Y. Chiao, Y. S. Wu, *Phys. Rev. Lett.* **1986**, *57*, 933.
[27] A. Tomita, R. Y. Chiao, *Phys. Rev. Lett.* **1986**, *57*, 2471.
[28] M. V. Berry, *Proc. R. Soc. London, Ser. A* **1984**, *392*, 45.
[29] Y. Qin, Y. Li, H. He, Q. Gong, *Opt. Lett.* **2009**, *34*, 2551.
[30] H. Luo, X. Ling, X. Zhou, W. Shu, S. Wen, D. Fan, *Phys. Rev. A* **2011**, *84*, 033801.
[31] W. J. M. Kort-Kamp, *Phys. Rev. Lett.* **2017**, *119*, 147401.
[32] L.-K. Shi, J. C. W. Song, *Phys. Rev. B* **2019**, *100*, 201405.
[33] M. Kim, D. Lee, J. Rho, *Laser Photonics Rev.* **2021**, *15*, 2100138.
[34] M. Yavorsky, E. Brasselet, *Opt. Lett.* **2012**, *37*, 3810.
[35] E. Brasselet, Y. Izdebskaya, V. Shvedov, A. S. Desyatnikov, W. Krolikowski, Y. S. Kivshar, *Opt. Lett.* **2009**, *34*, 1021.

[36] A. Ciattoni, A. Marini, C. Rizza, *Phys. Rev. Lett.* **2017**, *118*, 104301.
[37] X. Ling, F. Guan, X. Cai, S. Ma, H.-X. Xu, Q. He, S. Xiao, L. Zhou, *Laser Photonics Rev.* **2021**, *15*, 2000492.
[38] S. Pancharatnam, *Proc. - Indian Acad. Sci., Sect. A* **1956**, *44*, 398.
[39] M. V. Berry, *J. Mod. Opt.* **1987**, *34*, 1401.
[40] Z. Bomzon, V. Kleiner, E. Hasman, *Opt. Lett.* **2001**, *26*, 1424.
[41] L. Marrucci, C. Manzo, D. Paparo, *Phys. Rev. Lett.* **2006**, *96*, 163905.
[42] C. P. Jisha, S. Nolte, A. Alberucci, *Laser Photonics Rev.* **2021**, *15*, 2100003.
[43] Y. Guo, M. Pu, F. Zhang, M. Xu, X. Li, X. Ma, X. Luo, *Photonics Insights* **2022**, *1*, R03.
[44] C.-F. Li, *Phys. Rev. A* **2007**, *76*, 013811.
[45] A. Aiello, J. P. Woerdman, *Opt. Lett.* **2008**, *33*, 1437.
[46] X. Ling, H. Luo, F. Guan, X. Zhou, H. Luo, L. Zhou, *Opt. Express* **2020**, *28*, 27258.
[47] W. Zhu, H. Zheng, Y. Zhong, J. Yu, Z. Chen, *Phys. Rev. Lett.* **2021**, *126*, 083901.
[48] X. Ling, W. Xiao, S. Chen, X. Zhou, H. Luo, L. Zhou, *Phys. Rev. A* **2021**, *103*, 033515.
[49] A. Poddubny, I. Iorsh, P. Belov, Y. Kivshar, *Nat. Photonics* **2013**, *7*, 948.
[50] L. Ferrari, C. Wu, D. Lepage, X. Zhang, Z. Liu, *Prog. Quantum Electron.* **2015**, *40*, 1.
[51] D. Lee, S. So, G. Hu, M. Kim, T. Badloe, H. Cho, J. Kim, H. Kim, C.-W. Qiu, J. Rho, *eLight* **2022**, *2*, 1.